# Shell-model and Hartree-Fock calculations for even-mass O, Ne, and Mg nuclei

T. Siiskonen and P. O. Lipas
*Department of Physics, University of Jyväskylä, P.O. Box 35, FIN-40351 Jyväskylä, Finland*

J. Rikovska
*Department of Physics, Oxford University, Parks Road, Oxford OX1 3PU, United Kingdom*
*and Department of Chemistry, University of Maryland, College Park, Maryland 20742*
(Received 21 December 1998; published 24 August 1999)

Shell-model and deformed Hartree-Fock plus BCS calculations are reported for even-even nuclei $^{18-30}$O, $^{18-36}$Ne, and $^{20-42}$Mg; shell-model calculations additionally included $^{38,40}$Ne and $^{44,46,48}$Mg. Ground-state binding energies and $2_1^+$ quadrupole moments are calculated by both models. Shell-model calculations, aided by a new truncation method, include $2_1^+$ excitation energies and magnetic moments. Hartree-Fock calculations with SkI6, RATP, $Z_\sigma^*$, and SkX Skyrme forces include ground-state deformations and rms radii; SkI6 gives the best overall agreement with experiment. The two models are compared with each other and with experiment. Two-neutron separation energies, evidence for a neutron halo or skin in heavy O isotopes, and deformation of Ne and Mg isotopes are discussed. Both models indicate disappearance of the shell gap at $N=28$ (Mg), and the shell model does so additionally at $N=20$ (Ne and Mg). [S0556-2813(99)05109-2]

PACS number(s): 21.10.Dr, 21.10.Ky, 21.60.Cs, 21.60.Jz

## I. INTRODUCTION

The objective of the present study is to calculate and compare shell-model (SM) and Hartree-Fock (HF) results on even-even oxygen ($Z=8$), neon ($Z=10$), and magnesium ($Z=12$) nuclei in the mass range $A=18$–48. This region offeres a unique opportunity to carry out both SM and HF calculations up to and beyond the two-neutron drip line. The capabilities of the two models can be combined to provide a comprehensive description of nuclear low-energy properties.

Mean-field methods have been applied to the nuclear many-body problem for decades. In a qualitative and summary way, the original single-particle SM of 1949 [1] is a mean-field model. Subsequent development of the model has included first two and then several interacting valence nucleons in the mean field of a passive core of closed shells.

Following early work on valence nucleons in the $1p$ shell by Cohen and Kurath [2], Wildenthal and Brown and their associates have made a thorough study of $2s1d$ nuclei since the 1980's [3]. Similar work by Brown's group is now extended to the $1f2p$ shell [4]. In this line of work, the SM is applied as a numerical scheme with phenomenological input. No explicit mean field is assumed or derived; the single-particle energies (SPE) are taken from fits to experimental data. Also the effective interactions between the valence particles are taken as two-body matrix elements (TBME) obtained from the same fits. The resulting Hamiltonian matrix for the problem with many valence nucleons is diagonalized in a basis as large as is practically possible.

In the present work we follow Warburton *et al.* [5,6], whose SM space combines the $sd$ and $fp$ shells. Our calculations extend their O-Ne-Mg results [6] from $N=24$ to $N=36$. With enhanced computing power and a new efficient truncation method [7], we have also recalculated some of the earlier cases in larger SM spaces to present uniform systematics. Our calculations parallel the recent work of Caurier *et al.* [8], with a different SM space and effective interaction; detailed comparisons will be made below.

Nuclear Hartree-Fock (HF) calculations are modeled after atomic HF calculations; for a review of early work, see Ripka [9]. A HF calculation starts from an effective interaction and derives a mean field and a self-consistent set of SPEs. The most widely used effective interaction is the ten-parameter Skyrme force [10,11]. Its parameters are usually fitted to experimental properties of double-closed-shell nuclei.

When the Skyrme-HF model is applied to an open-shell nucleus, pairing must be included in the effective interaction. The simpler way is to add Bardeen-Cooper-Schrieffer (BCS) pairing to the Skyrme Hamiltonian; the more complicated, but theoretically more satisfactory, way is to include pairing self-consistently via a HF-Bogoliubov (HFB) calculation.

A HF calculation uses either a spherically symmetric (SHF) or deformed (DHF), axially symmetric or triaxial, mean field. The SPEs, the ground-state binding energy, and other ground-state properties, e.g., root-mean-square radii and static deformation parameters, are then calculated.

Our present HF application consists of axial DHF+BCS with Skyrme forces which have not been used in this region before. Indeed, very few nonrelativistic deformed HF calculations have been reported for even-even O-Ne-Mg nuclei. Tajima *et al.* [12] calculated $^{12-28}$O, $^{16-32}$Ne, and $^{18-38}$Mg using the SIII force, and Terasaki *et al.* [13] used the SIII and SLy4 forces to study $^{22-40}$Mg. Furthermore, the finite-range Gogny effective interaction was used in axial DHF calculations by Blumel and Dietrich [14] for selected even-even isotopes with $2\leqslant Z\leqslant 16$, and by Berger *et al.* [15] in a triaxial HFB model. Although many Skyrme parametrizations are known to give similar results for nuclei close to stability, it is of particular interest to extend their comparison to the particle drip lines.

The paper is organized as follows. Section II reports on SM calculations of ground-state binding energies and of $2_1^+$ excitation energies and quadrupole and magnetic moments.

 

Our HF calculations are described in Sec. III. Binding energies, proton and neutron deformations, and rms radii are calculated. The presence of a neutron skin or halo is investigated for heavy O isotopes, while deformations and mass radii are studied for Ne and Mg isotopes. In Sec. IV, we compare SM and HF, and Sec. V is a summary.

## II. SHELL-MODEL CALCULATIONS

### A. Interactions and truncations

We undertook SM calculations of even-even nuclei $^{18-30}$O, $^{18-40}$Ne, and $^{20-48}$Mg using the code OXBASH [16]. The basic configurations and important excitations of these nuclei occur in the $sd$–$fp$ shell. Accordingly, we chose our model space to include all single-particle (SP) orbits of the $sd$ and $fp$ shells. In this region isospin is a rather good quantum number, so we performed the calculations in the isospin formalism. The practical advantage of this is that calculations are reduced to manageable size.

Notable examples of earlier SM works in this mass region, especially on the so-called island of inversion, are Refs. [17] ($sd$–$f_{7/2}$ shell gap), [18] (beta decay near $N=20$), [8,19] (role of intruder configurations around $N=20$ and 28), and [20] (deformation of $^{32}$Mg).

The interaction was taken from Warburton, Becker, and Brown [6] (WBB). That interaction, designated WBMB, consists of four separate parts. The $sd$ part is the highly successful USD fit by Wildenthal [21]. It has constant SPEs, but its TBMEs have a mass dependence $(A-\nu)^{-0.3}$ when the valence space is $(sd)^{A-16-\nu}(fp)^{\nu}$. The $fp$ part is McGrory's fit [22]. The cross-shell matrix elements were generated from the Millener-Kurath potential [23] as modified by WBB. The last part of WBMB is a center-of-mass correction.

For a given symmetry characterized by $J^{\pi}T$, the excitations from the $sd$ to the $fp$ shell are in our work restricted to $n\hbar\omega$ excitations with a single value of $n$, where $n$ is the number of particles lifted from the $sd$ shell [24]. This is because the WBMB interaction is so devised that a single $n$ value is presupposed for any one calculation. In our calculations only one or two lowest possible values of $n$, for a given parity, were considered. Denoting the smallest $n$ by $n_0$, we are thus concerned with calculations characterized by $n=n_0$ and $n=n_0+2$.

Because of the large dimensions involved, we had to truncate our basis in many cases. This was done by a procedure due to French and Ratcliff [25] and further developed by Horoi *et al.* [7]. The method works so that partitions (configurations) whose calculated $m$-scheme energy exceeds a user-determined limit are excluded from the SM basis.

In the $m$ scheme, a particular partition $k$ has a certain energy expectation value, or energy centroid, $E_k=H_{kk}$ and a corresponding width $\sigma_k=\sqrt{(H^2)_{kk}-E_k^2}$, which depend on the SPEs and TBMEs. Let $E_{\min}$ be the lowest energy centroid among the various partitions $k$. Partitions whose energy exceeds a certain $E_{\rm cut}$ are discarded. This cutoff energy is conveniently stated in terms of the average $\overline{\sigma}$ of the $\sigma_k$ (the $\sigma_k$ have a roughly constant value),

$$E_{\rm cut}=E_{\min}+a\overline{\sigma}, \tag{1}$$

where $a$ is a user-chosen parameter. Convergence problems inherent in the software and hardware limitations resulted in $a\approx 2$–3 in our calculations using the cutoff method. This truncation procedure is logically and physically consistent because it is based on partition energies for a particular Hamiltonian.

The maximal dimensions of the Hamiltonian matrix were kept about the same for the entire mass range: roughly 25 000 for the $JT$ and 240 000 for the unprojected $m$ basis of the $2^+$ states. For comparison, the maximum $JT$ dimension of WBB was restricted to about 11 000.

### B. Binding energies

Coulomb energies and the binding energy of the $^{16}$O core must be included when we wish to calculate binding energies in the isospin formalism. The binding energy for $Z=9$–20 is then given by [6,26]

$$E_B=-E_{\rm g.s.}(T)+\Delta_C(Z), \tag{2}$$

where

$$\Delta_C(Z)=E_B(^{16}\mathrm{O})+(18\,247.80-950.495Z -162.025Z^2+45.29\delta_{Z,\rm odd})\ \text{keV}. \tag{3}$$

This equation contains the experimental binding energy $E_B(^{16}\mathrm{O})=127\,620$ keV, which is used for all O isotopes without the additional terms of Eq. (3). The energy $E_{\rm g.s.}(T)$ is the ground-state energy, with respect to the $^{16}$O core, calculated by the SM in isospin formalism. The calculated binding energy to be compared with experiment is then $E_B$.

The ground state was found to be given by $n=n_0$ in nearly all cases considered in this work, i.e., $E_B(n_0)>E_B(n_0+2)$. The exception is the region called the island of inversion in WBB. The first excited state came out as $2^+$ except for $^{28}$O, where it was $3^-$ (like the second excited state of $^{16}$O). This exception follows from the doubly magic nature of $^{28}$O: the ground state is of $0\hbar\omega$ character while the lowest excited states must be $n=1$ giving rise to negative parity and possible $J=3$.

The calculations of WBB are identical to ours when the same restrictions are used. However, we extend the calculations further to the neutron-rich side, with much larger matrix dimensions (we do not use their weak-coupling approximation). The binding energies of the $sd$-shell nuclei calculated with the WBMB Hamiltonian are identical to those predicted by the USD since $n=0$. According to our calculations, $^{30}$Ne and $^{32}$Mg are on the island of inversion, where the ground state is of $(n_0+2)\hbar\omega$ character.

Because of computational limitations, it was not possible in all cases to calculate higher $n\hbar\omega$ excitations. The nuclei for which it *was* reasonably possible are $^{28,30}$O, $^{30,32}$Ne, and $^{30,32}$Mg. However, the weak-coupling results of WBB show that for other O, Ne, and Mg nuclei $E_B(n_0)>E_B(n_0+2)$; the only exception is $^{34}$Mg.

In Table I the value of $n$ is given. Some of the $(n_0+2)\hbar\omega$ energies which are not listed in Table I can be found in Figs. 4 and 5 (weak coupling) of WBB. From Table I we

TABLE I. Results of shell-model calculations. Column 2 gives the $n$ of $n\hbar\omega$.

| | $n$ | $E_B$ (MeV) | $E(2_1^+)$ (MeV) | $Q(2_1^+)$ ($e$ fm$^2$) | $\mu(2_1^+)$ ($\mu_N$) |
|---|---|---|---|---|---|
| $^{18}_{8}O_{10}$ | 0 | 139.791 | 2.179 | −2.08 | −0.483 |
| $^{20}_{8}O_{12}$ | 0 | 151.444 | 1.962 | −3.25 | −0.512 |
| $^{22}_{8}O_{14}$ | 0 | 162.242 | 3.376 | 2.99 | −0.393 |
| $^{24}_{8}O_{16}$ | 0 | 168.669 | 4.180 | −2.35 | −0.138 |
| $^{26}_{8}O_{18}$ | 0 | 169.664 | 2.327 | 0.81 | 0.758 |
| $^{28}_{8}O_{20}$ | 0 | 168.879 | [a] | [a] | [a] |
| | 2 | 165.923 | 1.632 | −2.89 | −0.206 |
| $^{30}_{8}O_{22}$ | 2 | 164.484 | 1.761 | −3.38 | −0.385 |
| | 4 | 161.578 | 1.399 | −4.90 | −0.173 |
| $^{18}_{10}Ne_8$ | 0 | 132.331 | 2.179 | −8.01 | 2.525 |
| $^{20}_{10}Ne_{10}$ | 0 | 160.652 | 1.776 | −13.45 | 1.006 |
| $^{22}_{10}Ne_{12}$ | 0 | 177.764 | 1.368 | −13.15 | 0.745 |
| $^{24}_{10}Ne_{14}$ | 0 | 191.823 | 2.145 | −3.50 | 1.486 |
| $^{26}_{10}Ne_{16}$ | 0 | 201.785 | 2.011 | −10.26 | 1.786 |
| $^{28}_{10}Ne_{18}$ | 0 | 207.726 | 1.786 | −1.20 | 2.119 |
| $^{30}_{10}Ne_{20}$ | 0 | 210.126 | 1.883 | −0.94 | 2.888 |
| | 2 | 210.913 | 1.005 | −12.80 | 0.679 |
| $^{32}_{10}Ne_{22}$ | 2 | 212.224 | 1.105 | −11.89 | 0.781 |
| | 4[b] | 210.704 | 0.784 | −15.08 | 0.564 |
| $^{34}_{10}Ne_{24}$ | 4 | 212.751 | 0.834 | −16.29 | 0.635 |
| $^{36}_{10}Ne_{26}$ | 6 | 210.941 | 0.927 | −15.02 | 0.622 |
| $^{38}_{10}Ne_{28}$ | 8[b] | 207.548 | 1.006 | −5.43 | [c] |
| $^{40}_{10}Ne_{30}$ | 10[b] | 203.743 | 1.144 | −1.32 | 0.701 |
| $^{20}_{12}Mg_8$ | 0 | 134.954 | 1.962 | −12.52 | 2.566 |
| $^{22}_{12}Mg_{10}$ | 0 | 168.734 | 1.368 | −15.37 | 1.268 |
| $^{24}_{12}Mg_{12}$ | 0 | 198.209 | 1.508 | −16.36 | 1.007 |
| $^{26}_{12}Mg_{14}$ | 0 | 216.661 | 1.929 | −12.46 | 1.610 |
| $^{28}_{12}Mg_{16}$ | 0 | 231.659 | 1.543 | −15.32 | 1.216 |
| $^{30}_{12}Mg_{18}$ | 0 | 242.059 | 1.671 | −12.06 | 1.779 |
| | 2[b] | 236.012 | 1.131 | −12.36 | 0.602 |
| $^{32}_{12}Mg_{20}$ | 0 | 248.352 | 1.675 | −11.13 | 2.703 |
| | 2[b] | 248.861 | 1.046 | −13.85 | 0.755 |
| $^{34}_{12}Mg_{22}$ | 2 | 254.488 | 1.173 | −14.15 | 1.152 |
| $^{36}_{12}Mg_{24}$ | 4 | 259.303 | 0.797 | −18.70 | 0.750 |
| $^{38}_{12}Mg_{26}$ | 6[b] | 260.412 | 0.753 | −17.57 | 0.795 |
| $^{40}_{12}Mg_{28}$ | 8[b] | 261.167 | 0.701 | −18.68 | 0.590 |
| $^{42}_{12}Mg_{30}$ | 8[b] | 261.013 | 0.875 | −11.19 | [c] |
| $^{44}_{12}Mg_{32}$ | 8[b] | 261.365 | 1.349 | −4.86 | 1.194 |
| $^{46}_{12}Mg_{34}$ | 8[b] | 260.581 | 1.622 | −16.47 | 2.309 |
| $^{48}_{12}Mg_{36}$ | 8 | 255.319 | 1.255 | −7.66 | 1.371 |

[a]No $2^+$ state from $0\hbar\omega$ calculation.

[b]Restricted calculation.

[c]Calculation could not be carried out.

observe that $^{26}$O, $^{34}$Ne, and $^{40}$Mg are the last isotopes stable against two-neutron emission, as indicated by their maximal binding energy. The very recent SM calculations of Caurier *et al.* [8] give $^{24}$O, $^{34}$Ne, and $^{38}$Mg as the last bound isotopes. Fauerbach *et al.* [27] point out the model sensitivity of SM predictions regarding the stability of $^{26}$O.

The error in the binding energy increases when we exclude high-energy partitions by the Horoi truncation method [7]. The error has its maximum value around $N=30$ and it decreases when $N$ approaches the $fp$ shell closure at $N=40$ (in fact, we were able to calculate $^{48}$Mg without restrictions). The restricted calculations are so marked in Table I.

Our $2_1^+$ excitation energies (Table I) can be compared with those of Caurier *et al.* [8]. Their results are in close agreement with our $n=n_0$ results. The only exceptions occur at $N=28$, where our energies are appreciably lower than theirs, indicating less of a shell closure. The general congruence of the results, however, bears witness to the efficiency of our truncation procedure, since the $m$ dimension of Ref. [8] is about 30 times ours.

TABLE II. Quadrupole moments and magnetic moments of $2_1^+$ states calculated by the shell model, and Hartree-Fock quadrupole moments from Table III, compared with experiment [28].

| | $Q(e$ fm$^2)$ | | | $\mu$ ($\mu_N$) | |
|---|---|---|---|---|---|
| | SM | HF | Expt. | SM | Expt. |
| $^{18}$O | −2.08 | 0.00 | −3.6(9) | −0.483 | −0.57(3) |
| $^{20}$O | −3.25 | 0.00 | | −0.512 | −0.70(3) |
| $^{20}$Ne | −13.45 | −6.02 | −23(3) | 1.006 | 1.08(8) |
| $^{22}$Ne | −13.15 | −5.65 | −19(4) | 0.745 | 0.65(2) |
| $^{24}$Mg | −16.36 | −9.59 | −16.6(6) | 1.007 | 1.02(4) |
| $^{26}$Mg | −12.46 | 1.00 | −13.5(20) | 1.610 | 1.0(3) |

### C. Electromagnetic moments

The electromagnetic moments of the very neutron-rich, unstable nuclei considered in this work are not experimentally known [28]. For a detailed study of the dipole and quadrupole moments in the $sd$ shell, see Refs. [29,30]. In this work we extend the systematics.

The calculation of electromagnetic moments is implemented in the OXBASH package. We use effective charges $e_\pi=1.35e$ and $e_\nu=0.35e$, which have been found optimal for the $sd$ shell [31]. For the orbital $g$ factors we use the free-nucleon values, $g_{l\pi}=1$ and $g_{l\nu}=0$, while we quench the spin $g$ factors by the conventional factor of 0.7. The effective charges and $g$ factors represent summary corrections for mesonic effects and the finiteness of the model space.

Table I shows our SM results for the electromagnetic moments of $2_1^+$ states. Notable general features are the small, negative and positive, quadrupole moments of the O isotopes and the large negative quadrupole moments of most Ne and Mg isotopes. Experimental quadrupole moments are available [28] only for the stable isotopes $^{18}$O, $^{20,22}$Ne, and $^{24,26}$Mg. These nuclei, and additionally $^{20}$O, also have experimentally known magnetic moments [28]. The experimental and SM electromagnetic moments are listed in Table II for easy comparison. Agreement is seen to be good. The HF quadrupole moments shown will be discussed in Sec. IV.

The Ne and Mg nuclei in Table II have large negative quadrupole moments and thus are interpreted as prolate deformed in a Bohr-Mottelson description [32]. In that descrip-

tion, their $2_1^+$ magnetic moments are $\mu \approx (Z/A) \times 2\ \mu_N$. The values in the table are consistent with this.

Comparison of our $n=0$ quadrupole moments with the older $sd$-shell calculations [30] shows excellent agreement. This is to be expected since we have the same model space and the same interaction for the $sd$ shell. However, Carchidi *et al.* [30] only calculated the experimentally known cases (with two exceptions). As in the case of excitation energies, our $n=n_0$ results for the quadrupole moments closely agree with those of Caurier *et al.* [8].

For Ne and Mg the region around $N=24$, i.e., mid-shell between $N=20$ and $N=28$, seems to be strongly deformed according to Table I. The $2_1^+$ excitation energies drop below 1 MeV and the quadrupole moments have the largest negative values. Note also that $^{30}$Ne and $^{32}$Mg with $N=20$ have $(n_0+2)\hbar\omega$ ground states, small $2_1^+$ excitation energies, and large negative quadrupole moments. This implies that the $N=20$ shell gap has vanished, as has been recognized for a long time [33,34]. Furthermore, $^{40}$Mg with $N=28$ also has a small $2_1^+$ excitation energy and a large negative quadrupole moment, which indicates a collapse of the shell gap at $N=28$. This is surprising in view of a SM interpretation of $^{44}_{16}S_{28}$ which does indicate magic properties [35].

## III. HARTREE-FOCK CALCULATIONS

Ground-state properties of $^{18-30}$O, $^{18-36}$Ne, and $^{20-42}$Mg were calculated using the DHF+BCS model with axial symmetry using the computer code by Reinhard [36]. Both absolute total-energy minima and potential-energy surfaces were obtained. The coupled static mean-field equations were solved on a grid in coordinate space. Details of the numerical technique are given in Ref. [37].

Pairing was treated in the BCS formalism, using a zero-range state-dependent pairing force with different strengths for protons and neutrons. These strengths are adjusted for each Skyrme force individually, because pairing is treated as level-density dependent and is thus different for different Skyrme parametrizations. Details of the procedure can be found in Ref. [38].

The DHF+BCS calculations gave no indication of deformation for the oxygen ground states. We therefore carried out their further study in the spherical regime, using Reinhard's SHF+BCS code [39]. That gave us a handle on spherical SP states, crucial in the discussion of Sec. III A.

The Skyrme parametrizations used in the present study were SkI6 [40], RATP [41], $Z_\sigma^*$ [42], and the very new SkX [43]. The SkX force was fitted in the original work of Brown [43] without the pairing interaction. To use SkX for open-shell nuclei, we fitted the pairing strength parameters $V_0$ [38] to 20 spherical nuclei across the periodic table, with the result $V_{0\pi}=-249.5$ MeV fm$^3$ and $V_{0\nu}=-223.7$ MeV fm$^3$. However, the SkI6 force gave the best overall agreement with experiment in the O-Ne-Mg region, and we present mainly results obtained with this force. Some data based on the other Skyrme forces are quoted for comparison.

Our main HF results, obtained with the SkI6 Skyrme force, are collected in Table III. It gives ground-state binding energies, quadrupole deformation parameters for protons ($\beta_\pi$) and neutrons ($\beta_\nu$), rms charge radii $\overline{r}_{\rm ch} \equiv \langle r_{\rm ch}^2 \rangle^{1/2}$, and spectroscopic quadrupole moments.

TABLE III. Hartree-Fock results, obtained in DHF with the SkI6 Skyrme interaction. The spectroscopic quadrupole moments are subject to the constraints of the Bohr-Mottelson model as explained in the text.

| | $E_B$ (MeV) | $\beta_\pi$ | $\beta_\nu$ | $\overline{r}_{\rm ch}$ (fm) | $Q(2_1^+)$ ($e$ fm$^2$) |
|---|---|---|---|---|---|
| $^{18}_{8}O_{10}$ | 140.89 | 0.00 | 0.00 | 2.767 | 0.00 |
| $^{20}_{8}O_{12}$ | 151.25 | 0.00 | 0.00 | 2.765 | 0.00 |
| $^{22}_{8}O_{14}$ | 160.38 | 0.00 | 0.00 | 2.771 | 0.00 |
| $^{24}_{8}O_{16}$ | 167.87 | 0.00 | 0.00 | 2.786 | 0.00 |
| $^{26}_{8}O_{18}$ | 170.23 | 0.00 | 0.00 | 2.838 | 0.00 |
| $^{28}_{8}O_{20}$ | 173.37 | 0.00 | 0.00 | 2.889 | 0.00 |
| $^{30}_{8}O_{22}$ | 171.45 | 0.00 | 0.33 | 2.887 | 0.00 |
| $^{18}_{10}Ne_{8}$ | 133.67 | 0.00 | 0.00 | 3.011 | 0.00 |
| $^{20}_{10}Ne_{10}$ | 157.29 | 0.38 | 0.37 | 3.009 | −6.02 |
| $^{22}_{10}Ne_{12}$ | 176.15 | 0.33 | 0.34 | 2.971 | −5.65 |
| $^{24}_{10}Ne_{14}$ | 189.40 | −0.22 | −0.23 | 2.956 | 2.99 |
| $^{26}_{10}Ne_{16}$ | 199.93 | 0.20 | 0.16 | 2.961 | −3.81 |
| $^{28}_{10}Ne_{18}$ | 207.41 | 0.17 | 0.10 | 2.999 | −3.44 |
| $^{30}_{10}Ne_{20}$ | 214.83 | 0.00 | 0.00 | 3.034 | 0.00 |
| $^{32}_{10}Ne_{22}$ | 214.39 | 0.32 | 0.26 | 3.105 | −7.92 |
| $^{34}_{10}Ne_{24}$ | 214.95 | 0.40 | 0.32 | 3.135 | −10.86 |
| $^{36}_{10}Ne_{26}$ | 213.84 | 0.38 | 0.55 | 3.147 | −10.77 |
| $^{20}_{12}Mg_{8}$ | 135.78 | 0.00 | 0.00 | 3.191 | 0.00 |
| $^{22}_{12}Mg_{10}$ | 168.17 | 0.40 | 0.41 | 3.155 | −8.51 |
| $^{24}_{12}Mg_{12}$ | 195.15 | 0.41 | 0.41 | 3.126 | −9.59 |
| $^{26}_{12}Mg_{14}$ | 213.59 | −0.05 | −0.05 | 3.029 | 1.00 |
| $^{28}_{12}Mg_{16}$ | 229.27 | 0.34 | 0.27 | 3.118 | −8.97 |
| $^{30}_{12}Mg_{18}$ | 240.94 | −0.15 | −0.13 | 3.107 | 3.28 |
| $^{32}_{12}Mg_{20}$ | 252.73 | 0.00 | 0.00 | 3.171 | 0.00 |
| $^{34}_{12}Mg_{22}$ | 256.00 | 0.32 | 0.24 | 3.200 | −10.06 |
| $^{36}_{12}Mg_{24}$ | 261.17 | 0.40 | 0.31 | 3.247 | −13.73 |
| $^{38}_{12}Mg_{26}$ | 262.81 | 0.39 | 0.33 | 3.266 | −13.99 |
| $^{40}_{12}Mg_{28}$ | 264.46 | 0.39 | 0.32 | 3.292 | −14.64 |
| $^{42}_{12}Mg_{30}$ | 263.64 | 0.29 | 0.18 | 3.290 | −10.90 |

Quadrupole moments [and $B(E2)$ values] can be obtained by HF only through the auxiliary mechanism of the Bohr-Mottelson rotational model [32]. Since that model is applicable only to nuclei with well-defined large deformations, the results for $Q(2_1^+)$ in Table III are quantitatively significant only for such nuclei. For an axially symmetric quadrupole-shaped nucleus with a large deformation and diffuse surface, the Bohr-Mottelson intrinsic quadrupole moment is [32]

$$Q_0 = \frac{3}{\sqrt{5\pi}} Z e R_0^2 \beta_\pi \left[ 1 + \sqrt{\frac{20}{49\pi}} \beta_\pi - \frac{4\pi^2}{3} \left( \frac{a_0}{R_0} \right)^2 \right]. \quad (4)$$

For $R_0$ and $a_0$ we use the standard values $1.2A^{1/3}$ fm and 0.6 fm. In the present application the second and third terms,

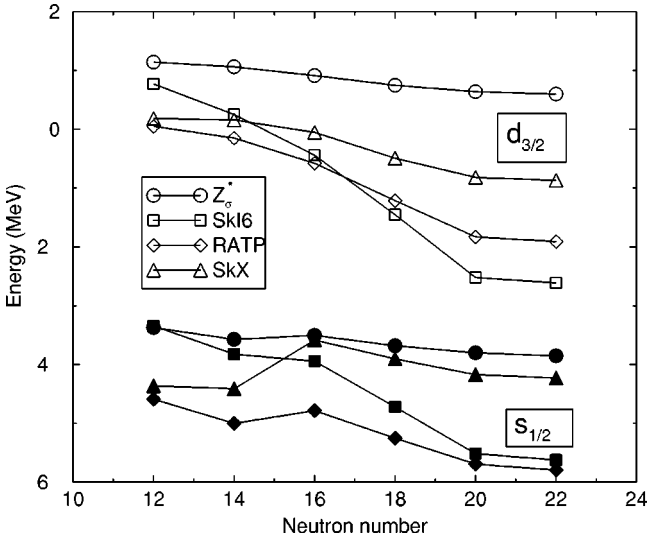


FIG. 1. Hartree-Fock neutron single-particle energies calculated with various Skyrme forces.

usually omitted, diminish $|Q_0|$ typically by 25%. The Bohr-Mottelson spectroscopic quadrupole moment, given in the last column of Table III, is $Q(2_1^+) = -\frac{2}{7}Q_0$.

Applications of our results to some important phenomena in the O-Ne-Mg region are discussed below.

### A. Heavy oxygen isotopes

#### *1. The neutron drip line*

For calculations of ground-state properties of even-even oxygen isotopes, a main point of interest is the location of the two-neutron drip line. The heaviest experimentally known O isotope is $^{24}$O. Recent experimental efforts to produce $^{26}$O [27,44] and $^{28}$O [45] have not been successful.

There are numerous theoretical predictions of particle stability of the neutron-rich O nuclei. They are based on the SM [27,46], spherical Skyrme-HF [47], relativistic mean-field theory (RMF) [48], and the finite-range droplet model (FRDM) [49]. Global systematics and extrapolation of experimental masses by Audi *et al.* [50] indicate that the heaviest O isotope stable against particle emission is $^{24}$O, while the FRDM predicts that even $^{26}$O and $^{28}$O are stable. The latter results agree with predictions by Shen and Ren [47] using the SkI4 force, and by Ren *et al.* [48] using the RMF.

Our SM predicts two-neutron stability of $^{26}$O. Our various HF calculations predict the heaviest particle-stable O isotope either at $A=24$ ($Z^*_\sigma$) or at $A=28$ (SkI6, RATP, and SkX). The latter result agrees with Nayak and Sapathy's work [51] with SI-SIV Skyrme forces. The difference in HF predictions can be understood from neutron SPEs as follows.

We compare in Fig. 1 the neutron-number dependence of the $d_{3/2}$ and $s_{1/2}$ energies for different Skyrme forces. The crucial difference between the forces is that for $16 \leqslant N \leqslant 20$ the $d_{3/2}$ orbital is bound for SkI6, RATP, and SkX, but unbound for $Z^*_\sigma$. Therefore, when this orbital starts to fill (pairwise) at $N=18$, it leads to particle instability in the case of $Z^*_\sigma$, but leaves $N=18$ and $N=20$ stable for the other forces.

TABLE IV. Hartree-Fock results (SkI6) for heavy oxygen isotopes. Column 2: neutron pairing energies; column 3: difference between rms radii of neutron and proton distributions; column 4: occupation of continuum states. Columns 5–8 give properties of neutron $sd$ single-particle states: energy, rms radius, occupation.

| | $E_{\rm pair}$ (MeV) | $\delta\overline{r}$ (fm) | $N_{\rm cont}$ | Orbital | $\epsilon$ (MeV) | $\overline{r}_{\rm sp}$ (fm) | $N_{\rm sp}$ |
|---|---|---|---|---|---|---|---|
| $^{20}_{8}O_{12}$ | −3.01 | 0.35 | 0.034 | $d_{5/2}$ | −5.45 | 4.27 | 3.851 |
| | | | | $s_{1/2}$ | −3.34 | 5.79 | 0.145 |
| | | | | $d_{3/2}$ | 0.77 | 9.09 | 0.034 |
| $^{22}_{8}O_{14}$ | −1.42 | 0.46 | 0.029 | $d_{5/2}$ | −5.58 | 4.29 | 5.499 |
| | | | | $s_{1/2}$ | −3.82 | 5.66 | 0.484 |
| | | | | $d_{3/2}$ | 0.25 | 7.74 | 0.028 |
| $^{24}_{8}O_{16}$ | 0.00 | 0.62 | 0.000 | $d_{5/2}$ | −6.51 | 4.28 | 6.000 |
| | | | | $s_{1/2}$ | −3.94 | 5.71 | 2.000 |
| | | | | $d_{3/2}$ | −0.44 | 6.56 | 0.000 |
| $^{26}_{8}O_{18}$ | −0.94 | 0.71 | 0.000 | $d_{5/2}$ | −7.17 | 4.30 | 5.966 |
| | | | | $s_{1/2}$ | −4.72 | 5.53 | 1.985 |
| | | | | $d_{3/2}$ | −1.45 | 5.75 | 2.048 |
| $^{28}_{8}O_{20}$ | 0.00 | 0.73 | 0.000 | $d_{5/2}$ | −7.88 | 4.31 | 6.000 |
| | | | | $s_{1/2}$ | −5.51 | 5.40 | 2.000 |
| | | | | $d_{3/2}$ | −2.52 | 5.31 | 4.000 |

For SkI6, RATP, and SkX, two-neutron instability does not occur until $N=22$ when the unbound $f_{7/2}$ starts to fill. SPE behavior for different Skyrme parametrizations is hard to control far from stability. This is one of the reasons why it is difficult to make accurate HF predictions far from stability.

#### *2. Neutron halo or skin?*

Halos result from the presence of a bound state close to the continuum (for a recent review, see, e.g., Ref. [52]). A combination of a low separation energy and low angular momentum, together with the short range of the nuclear force, allows one or more nucleons to tunnel far beyond the normal nuclear radius and be present there with an appreciable probability. The separation energies of the last neutron(s) in the well-known halo systems $^{11}$Li, $^{11}$Be, and $^{6}$He are 0.3, 0.5, and 0.97 MeV, respectively, and the halo-neutron orbitals are $2s$ and $1p$. The halo appears as a density tail at 5 fm $\lesssim r \lesssim$ 10 fm, where the density is only about 1/100 of the density in the center of the nucleus [53].

Based on RMF calculations, Ren *et al.* [48] have reported multineutron halos in $^{24-28}$O. Their conclusion relies on enhanced rms radii of the $2s_{1/2}$ and $1d_{3/2}$ neutron SP states; our SP radii (Table IV) behave similarly. However, their conclusion is not supported by the multineutron binding energies, which are much too high ($\lesssim$10 MeV) by all accounts, including their own results and ours as well as experiment (see Table V). Moreover, halo formation is not favored by the high orbital angular momentum of the $1d_{3/2}$ state.

We have thus established that there is hardly a case for a neutron halo in the heavy O isotopes and proceed to explore the possibility of another drip-line phenomenon, namely the neutron skin.

TABLE V. Comparison of the shell-model, Hartree-Fock (SkI6), and experimental [50] binding energies.

| | $E_B$ (MeV) | | |
|---|---|---|---|
| | SM | HF | Expt. |
| $^{18}_{8}O_{10}$ | 139.791 | 140.89 | 139.803 |
| $^{20}_{8}O_{12}$ | 151.444 | 151.25 | 151.367 |
| $^{22}_{8}O_{14}$ | 162.242 | 160.38 | 162.027 |
| $^{24}_{8}O_{16}$ | 168.669 | 167.87 | 168.477 |
| $^{26}_{8}O_{18}$ | 169.664 | 170.23 | 168.430[a] |
| $^{18}_{10}Ne_{8}$ | 132.331 | 133.67 | 132.150 |
| $^{20}_{10}Ne_{10}$ | 160.652 | 157.29 | 160.641 |
| $^{22}_{10}Ne_{12}$ | 177.764 | 176.15 | 177.766 |
| $^{24}_{10}Ne_{14}$ | 191.823 | 189.06 | 191.832 |
| $^{26}_{10}Ne_{16}$ | 201.785 | 199.93 | 201.596 |
| $^{28}_{10}Ne_{18}$ | 207.726 | 207.41 | 206.889 |
| $^{30}_{10}Ne_{20}$ | 210.913 | 214.83 | 212.063 |
| $^{32}_{10}Ne_{22}$ | 212.224 | 214.39 | 213.272 |
| $^{20}_{12}Mg_{8}$ | 134.954 | 135.78 | 134.465 |
| $^{22}_{12}Mg_{10}$ | 168.734 | 168.17 | 168.574 |
| $^{24}_{12}Mg_{12}$ | 198.209 | 195.15 | 198.254 |
| $^{26}_{12}Mg_{14}$ | 216.661 | 213.59 | 216.678 |
| $^{28}_{12}Mg_{16}$ | 231.659 | 229.27 | 231.623 |
| $^{30}_{12}Mg_{18}$ | 242.059 | 240.94 | 241.627 |
| $^{32}_{12}Mg_{20}$ | 248.861 | 252.73 | 249.690 |
| $^{34}_{12}Mg_{22}$ | 254.488 | 256.00 | 256.580 |
| $^{36}_{12}Mg_{24}$ | 259.303 | 261.17 | 260.262 |

[a]Stated in Ref. [50] as an extrapolation of experimental values.

In their HF studies Fukunishi *et al.* [54] have suggested a quantitative definition of the skin in terms of the ratio of neutron and proton densities. Thus the inner boundary is determined by the radius $R_1$ for which $\rho_\nu(R_1)/\rho_\pi(R_1)=\xi_1$ where $\xi_1$ is a constant appreciably larger than $N/Z$, the expected density ratio in the nuclear interior. The outer skin boundary, marking the onset of the halo region, is defined by a radius $R_2$ for which $\rho_\nu(R_2)=\xi_2\rho_\nu(0)$ where $\rho_\nu(0)$ is the central neutron density. The skin thickness is defined as $\delta R = R_2 - R_1$ and the halo region as $r > R_2$.

From our calculated (SHF+BCS, SkI6) densities, and with the choice $\xi_1=5.0$ and $\xi_2=0.01$, we deduced $R_1$ and $R_2$. Figure 2 shows $\delta R$ (top panel) and the number of particles within the skin region (middle panel) as functions of $A$. It is clearly seen that the skin thickness and skin occupation grow monotonically with $N$. The number of nucleons in the halo region also grows monotonically with $A$, but remains well below unity in all cases.

The bottom panel of Fig. 2 is a plot of $\delta\bar{r} \equiv \bar{r}_\nu - \bar{r}_\pi$ vs the Fermi-energy difference $\Delta\epsilon_F \equiv \epsilon_F^\nu - \epsilon_F^\pi$. The systematics of Tanihata *et al.* [55] indicates that for $\Delta\epsilon_F \gtrsim 10$ MeV the difference $\delta\bar{r}$ is about 0.5 fm or greater, which is considered the criterion for the presence of a neutron skin. This criterion is seen to be well met by $^{24,26,28}$O. Table IV gives rms radii $\bar{r}_{\rm sp}$ for the neutron $sd$ orbitals. They are appreciably larger than the conventional nuclear radius $1.2A^{1/3}$ fm$\approx$3.5 fm. The table also shows the differences $\delta\bar{r}$.

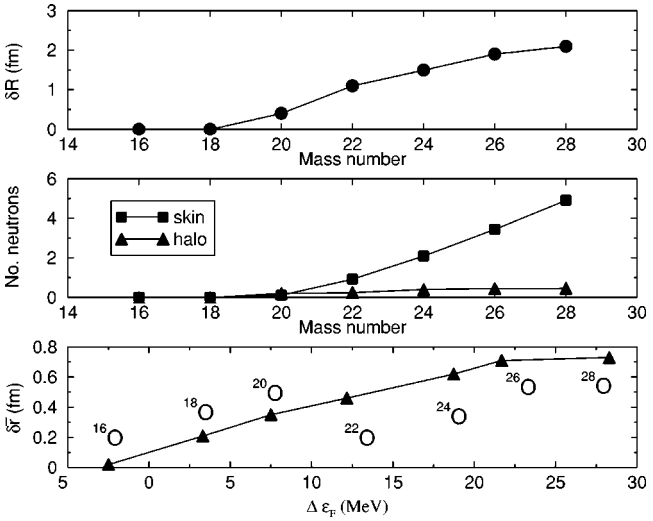


FIG. 2. Top: neutron-skin thickness $\delta R = R_2 - R_1$ (see text). Middle: number of neutrons in the skin of thickness $\delta R$ and in the halo ($r > R_2$). Bottom: difference $\delta\bar{r}$ of neutron and proton rms radii as a function of the difference $\Delta\epsilon_F$ of the neutron and proton Fermi energies.

It is well known [56] that HF+BCS models may produce incorrect nuclear radii close to particle drip lines because pairs of nucleons scatter into the continuum. To address this problem, we give in Table IV the $sd$-shell neutron occupation probabilities $N_{\rm sp}$ for $^{20-28}$O. From the table (and Fig. 1) we then see that the last significantly occupied orbital is well bound throughout the region. The table also shows directly that the number of particles in the continuum, $N_{\rm cont}$, is $\lesssim 0.03$ in all cases, and thus negligible. Therefore radii calculated in this work are not affected by nonphysical effects.

We conclude from the above considerations that our HF model predicts a neutron skin, but no halo, in $^{24,26,28}$O. Brown and Richter [34] have likewise predicted a neutron skin in neutron-rich Na isotopes.

### B. Ne and Mg isotopes: Shapes and magic numbers

The heaviest experimentally observed neon and magnesium isotopes are $^{32}$Ne [44] and $^{38}$Mg [57]. Our HF calculations with various Skyrme forces predict $^{30}$Ne or $^{34}$Ne as the last Ne isotope stable with respect to two-neutron emission; Table III (SkI6) shows that $^{30}$Ne and $^{34}$Ne are stable but $^{32}$Ne is not. All our HF calculations predict $^{40}$Mg as the last Mg isotope stable against two-neutron emission. Our respective SM predictions are $^{34}$Ne and $^{40}$Mg.

It is well known (cf. Table II) that some heavy Ne and Mg nuclei exhibit large deformations. Our HF results in Table III are in a very satisfactory overall agreement with those of the FRDM model [49] and recent RMF calculations [58]. As one would expect for the magic numbers $N=8$ and $N=20$, $^{18}$Ne and $^{30}$Ne, as well as $^{20}$Mg and $^{32}$Mg, come out spherical. We note from the table that $^{26}$Mg is nearly spherical, which coincides with the $d_{5/2}$ subshell closure at $N=14$. Our only appreciable oblate deformations are for $^{24}$Ne and $^{30}$Mg, both in line with the FRDM predictions. Finally we note that we

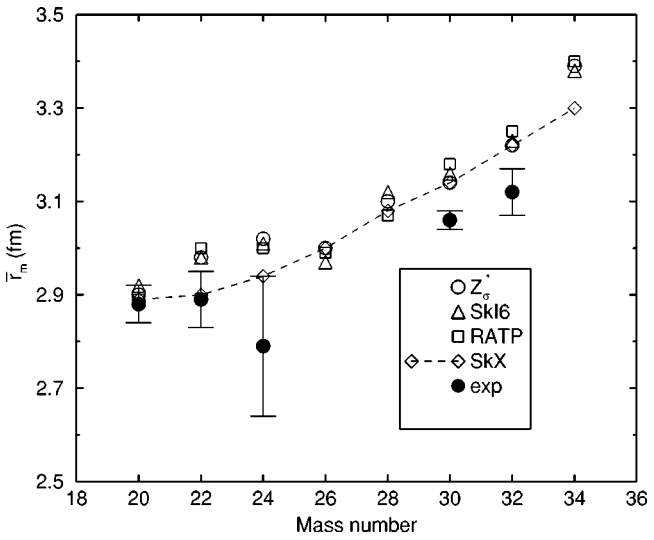


FIG. 3. Matter rms radii of Mg isotopes: calculated by Hartree-Fock with various Skyrme forces and experimental forces [62].

do not predict a spherical shape for $^{40}$Mg, which indicates a collapse of the magic number $N=28$.

Comparison of our deformation parameters in Table III with experimental deformations extracted from measured $B(E2)$ values on the Bohr-Mottelson description [59] shows that the shell effects discussed above are not fully supported by experiment. Experimental deformations for $^{18}$Ne, $^{26}$Mg, and $^{32}$Mg are $\beta \gtrsim 0.5$ [59,60], while our HF predictions are $\beta \approx 0$. The conflict indicates failure, in these cases, of the Bohr-Mottelson dynamics or of the HF results.

All HF calculations published so far (see, e.g., Refs. [12,13,15,61]), as well as the FRDM [49], predict the shape of $^{32}$Mg to be spherical, which appears as a natural response of the mean field to the $N=20$ shell closure. We have made further DHF tests with the four Skyrme forces used in this study. The results are similar in all cases: the principal minimum is always at $\beta=0$ and a secondary minimum occurs at $\beta \approx 0.3$–$0.4$. However, the secondary minimum deepens with decreasing pairing strength. With no pairing, $Z^*_\sigma$ produces the principal minimum at $\beta \approx 0.4$ and a secondary minimum at $\beta=0$.

Suzuki *et al.* [62] reported recently experimental effective rms matter radii of some Na and Mg nuclei. They concluded that the increase of the rms matter radius is mainly due to an increase of the rms neutron radius. The presence of a neutron skin was predicted in heavy Na and Mg nuclei. Spherical [54] and deformed [12] HF and RMF [63] models were used to calculate the mass-number dependence of matter radii in heavy even-even Mg.

We have also calculated the rms matter radii $\overline{r_m}$ of $^{20-34}$Mg by DHF with the various Skyrme parametrizations. The results are shown in Fig. 3 together with the experimental radii of Suzuki *et al.* All the Skyrme forces used overpredict the experimental data by $\lesssim 3\%$. On the whole, the agreement between theory and experiment is similar to that presented in Ref. [62].

## IV. COMPARISON BETWEEN SHELL MODEL AND HARTREE-FOCK

We first note the main qualitative differences between SM and HF. The SM produces nuclear eigenstates as admixtures, determined by the particle interactions, of Slater determinants. The HF model, on the other hand, produces the intrinsic ground state as a single Slater determinant. While the SM is used to calculate specific spectroscopic properties, HF yields global ground-state properties, particularly the binding energy and matter and charge distributions.

The essential input into HF consists of the effective interaction, selected to be of the Skyrme type in the present study. Single-particle energies are then predicted by the HF calculation. The SM input, on the other hand, consists of a complete numerical Hamiltonian expressed in terms of SPEs and TBMEs. Thus the WBMB Hamiltonian [6] used in our present SM application $(sd+fp)$ is stated in terms of 7 SPEs and 510 TBMEs; these numbers are from fits to experimental binding and excitation energies in the $sdfp$ region. Although SM and HF are usually kept apart as disparate disciplines, we note the recent work by Brown and Richter [64] where they are combined; in particular, SPEs from HF are used as input in SM.

The HF procedure produces the intrinsic nuclear shape within the constraints imposed: in the present case the axial quadrupole shape for protons and neutrons, with respective parameters $\beta_\pi$ and $\beta_\nu$. Spectroscopic quadrupole moments and $B(E2)$ values can then be obtained through the Bohr-Mottelson rigid-rotor model, when applicable. Conversely, SM results can be interpreted in terms of a nuclear shape only through the same prescription applied in reverse.

The SM and HF quadrupole moments are quite different even qualitatively. All oxygen isotopes have $Q=0$ by HF, while the SM values (Table I) are fairly small and mostly negative. All SM values for neon and magnesium are negative. The HF counterparts of most large negative SM quadrupole moments are also negative, but the HF results for Ne and Mg contain also zero and positive values. The HF results indicate validity of the magic numbers $N=8$ and 20, but not of 28. With the $^{16}$O core, the SM trivially contains $N=8$ as a magic number. As discussed in Sec. II C, $N=20$ for Ne and Mg, and $N=28$ for Mg do not display a magic SM character. Table II shows that the SM quadrupole moments are in much better agreement with experiment than are the HF ones; a HF failure occurs for $^{26}$Mg.

The nucleus $^{32}_{12}\mathrm{Mg}_{20}$, already discussed above, has received considerable attention recently [20,33,60]. For it, our HF gives zero deformation, whence $Q_0=0$. For the $2^+_1$ excitation probability the Bohr-Mottelson rotational scheme gives [32] $B(E2)\uparrow=(5/16\pi)e^2Q_0^2$, which then is zero in this case. However, this quantity has been measured and found to be large [60]: $454\pm78\ e^2\mathrm{fm}^4$. Our SM calculation gives 358 $e^2\mathrm{fm}^4$, which is in substantial agreement with the experimental value. The four-particle, four-hole SM result of Fukunishi *et al.* [33] is even better, 449 $e^2\mathrm{fm}^4$, but the difference is mostly due to different effective charges: with their effective charges we get 431 $e^2\mathrm{fm}^4$. Their $2^+_1$ excitation energy is 1.17 MeV, while ours is 1.046 MeV (Table I); the experi-

mental value is 0.885 MeV [60].

The binding energy is the only property on which we can make a *direct* comparison between our SM and HF results; for $E2$ properties HF needs the Bohr-Mottelson scheme. Table V gives our calculated binding energies together with their experimental counterparts where available [50]. Where Table I lists two $n$ values, i.e., $n_0$ and $n_0+2$, for a given nucleus, we adopt the greater value for the binding energy. That is the one for $n=n_0$ except for $^{30}$Ne and $^{32}$Mg. The exceptions lie on the island of inversion of WBB. However, $^{32}$Ne lies on their island of inversion but not on ours. This difference is evidently due to the fact that their calculation is based on a weak-coupling approximation while ours is a normal, although restricted, SM calculation. We also note that our agreement with them is within 3 keV except for $^{36}$Mg, where their value is about 5 MeV less than ours; the difference is evidently due to our much larger SM space for that nucleus.

When we compare the actual numerical values of our calculated binding energies with the experimental values (see Table V), we see that the SM values are mostly closer to experiment than are the HF values. This of course is not surprising because the numerical Hamiltonian (WBMB) used in our SM is the result of a fit to experimental binding energies and low excitation energies, whereas our HF Hamiltonian is the result of a much more global fit to data.

## V. SUMMARY

We have made shell-model and Hartree-Fock calculations of the even-even nuclei $^{18-30}$O, $^{18-40}$Ne, and $^{20-48}$Mg. Ground-state binding energies and $2_1^+$ quadrupole moments were calculated by both models. Additionally, $2_1^+$ excitation energies and magnetic moments were calculated by the SM, and deformations (protons and neutrons) and rms radii (charge and matter) by HF.

The SM calculations included all SP orbitals of the $sd$ and $fp$ shells. Where necessary, the many-particle space was restricted on the basis of configuration energies by a method developed by Horoi *et al.* [7]. Comparisons with other calculations indicate that this is an efficient cutoff method. The numerical Hamiltonian used is due to Warburton *et al.* [6].

Hartree-Fock calculations were made with Skyrme forces (SkI6 [40], RATP [41], $Z_\sigma^*$ [42], and SkX [43]) and BCS pairing. Most calculations were done with SkI6, which we judged to give the best overall agreement with experiment.

Our SM and HF (SkI6) calculations predicted nearly the same two-neutron drip lines, with $^{26,28}$O, $^{34}$Ne, and $^{40}$Mg as the last stable isotopes. Altogether, the SM and HF binding-energy predictions were within 2 MeV and 3 MeV, respectively, of the experimental values.

The SM and HF results on quadrupole moments were markedly different. Hartree-Fock gave zero quadrupole moments, i.e., spherical shapes, at magic numbers $N=8$ and 20, but not at $N=28$. The SM results of large negative quadrupole moments, together with low $2_1^+$ excitation energies, indicate that $N=20$ is not a magic number for $Z=10$ and 12, and that $N=28$ is not magic for $Z=12$. The nuclei $^{30}$Ne and $^{32}$Mg lie on the ''island of inversion.'' The SM quadrupole moments are in much better agreement with experiment than are the HF ones.

From our HF study of proton and neutron distributions and associated radii of the oxygen isotopes we conclude that $^{24-28}$O have neutron skins but not halos. Magnesium mass radii calculated by different Skyrme forces were close to each other and in good agreement with experiment.

## ACKNOWLEDGMENTS

We are most grateful to Alex Brown for a careful reading of the manuscript and subsequent advice. One of the authors (J.R.) thanks P.-G. Reinhard for his constant support and helpful discussions concerning the Hartree-Fock codes, and Paul Stevenson and Pontus Lurcock for help with running the codes. She acknowledges financial support from U.S. DOE Grant No. DE-FG02-94ER40834.

[1] O. Haxel, J. H. D. Jensen, and H. E. Suess, Phys. Rev. **75**, 1766 (1949); M. G. Mayer, *ibid.* **75**, 1969 (1949).
[2] S. Cohen and D. Kurath, Nucl. Phys. **73**, 1 (1965).
[3] B. A. Brown and B. H. Wildenthal, Annu. Rev. Nucl. Part. Sci. **38**, 29 (1988).
[4] M. G. van der Merwe, W. A. Richter, and B. A. Brown, Nucl. Phys. **A579**, 173 (1994).
[5] E. K. Warburton, D. E. Alburger, J. A. Becker, B. A. Brown, and S. Raman, Phys. Rev. C **34**, 1031 (1986).
[6] E. K. Warburton, J. A. Becker, and B. A. Brown, Phys. Rev. C **41**, 1147 (1990).
[7] M. Horoi, B. A. Brown, and V. Zelevinsky, Phys. Rev. C **50**, R2274 (1994).
[8] E. Caurier, F. Nowacki, A. Poves, and J. Retamosa, Phys. Rev. C **58**, 2033 (1998).
[9] G. Ripka, Adv. Nucl. Phys. **1**, 183 (1968).
[10] T. H. R. Skyrme, Nucl. Phys. **9**, 615 (1959).
[11] D. Vautherin and D. M. Brink, Phys. Rev. C **5**, 626 (1972).
[12] N. Tajima, S. Takahara, and N. Onishi, Nucl. Phys. **A603**, 23 (1996).
[13] J. Terasaki, H. Flocard, P.-H. Heenen, and P. Bonche, Nucl. Phys. **A621**, 706 (1997).
[14] R. Blumel and K. Dietrich, Nucl. Phys. **A471**, 453 (1987).
[15] J. F. Berger, J. P. Delaroche, M. Girod, S. Peru, J. Libert, and I. Deloncle, in *Nuclei Far From Stability/Atomic Masses and Fundamental Constants 1992*, edited by R. Neugart and A. Wöhr (IOP, Bristol, 1993), p. 487.
[16] B. A. Brown, A. Etchegoyen, and W. D. M. Rae, OXBASH, the Oxford University-Buenos Aires-MSU shell-model code, Michigan State University Cyclotron Laboratory Report No. 524, 1988.
[17] M. H. Storm, A. Watt, and R. R. Whitehead, J. Phys. G **9**, L165 (1983).

[18] G. Klotz, P. Baumann, M. Bounajma, A. Huck, A. Knipper, G. Walter, G. Marguier, C. Richard-Serre, A. Poves, and J. Retamosa, Phys. Rev. C **47**, 2502 (1993).
[19] A. Poves and J. Retamosa, Nucl. Phys. **A571**, 221 (1994).
[20] T. Otsuka, Nucl. Phys. **A616**, 406c (1997).
[21] B. H. Wildenthal, Prog. Part. Nucl. Phys. **11**, 5 (1984).
[22] J. P. McGrory, Phys. Rev. C **8**, 693 (1973).
[23] D. J. Millener and D. Kurath, Nucl. Phys. **A255**, 315 (1975).
[24] For $A \leqslant 40$, we have simply $n=\nu$. However, for $A>40$ the $sd$ shell cannot accommodate all the particles for any isospin, and we have $n=\nu-(A-40)$. In the present work this latter condition occurs only for $^{42,44,46,48}$Mg, all of which have $n=8$; see Table I.
[25] J. B. French and K. F. Ratcliff, Phys. Rev. C **3**, 94 (1971).
[26] W. Chung, Ph.D. thesis, Michigan State University, 1976.
[27] M. Fauerbach, D. J. Morrissey, W. Benenson, B. A. Brown, M. Hellström, J. H. Kelley, R. A. Kryger, R. Pfaff, C. F. Powell, and B. M. Sherrill, Phys. Rev. C **53**, 647 (1996).
[28] R. B. Firestone, V. S. Shirley, S. Y. F. Chu, C. M. Baglin, and J. Zipkin, *Table of Isotopes CD-ROM*, 8th ed., Version 1.0 (Wiley-Interscience, New York, 1996).
[29] B. A. Brown and B. H. Wildenthal, Phys. Rev. C **28**, 2397 (1983).
[30] M. Carchidi, B. H. Wildenthal, and B. A. Brown, Phys. Rev. C **34**, 2280 (1986).
[31] B. A. Brown, B. H. Wildenthal, W. Chung, S. E. Massen, M. Bernas, A. M. Bernstein, R. Miskimen, V. R. Brown, and V. A. Madsen, Phys. Rev. C **26**, 2247 (1982).
[32] A. Bohr and B. R. Mottelson, *Nuclear Structure* (Benjamin, New York, 1975), Vol. II.
[33] N. Fukunishi, T. Otsuka, and T. Sebe, Phys. Lett. B **296**, 279 (1992).
[34] B. A. Brown and W. A. Richter, Phys. Rev. C **54**, 673 (1996).
[35] T. Glasmacher, B. A. Brown, M. J. Chromik, P. D. Cottle, M. Fauerbach, R. W. Ibbotson, K. W. Kemper, D. J. Morrisey, H. Scheit, D. W. Sklenica, and M. Steiner, Phys. Lett. B **395**, 163 (1997).
[36] P.-G. Reinhard (private communication).
[37] V. Blum, G. Lauritsch, J. A. Maruhn, and P.-G. Reinhard, J. Comput. Phys. **100**, 364 (1992).
[38] P.-G. Reinhard, W. Nazarewicz, M. Bender, and J. A. Maruhn, Phys. Rev. C **53**, 2776 (1996); M. Bender, P.-G. Reinhard, K. Rutz, and J. A. Maruhn, Phys. Rev. C (submitted).
[39] P.-G. Reinhard, in *Computational Nuclear Physics 1*, edited by K. Langanke, J. A. Maruhn, and S. E. Koonin (Springer, Berlin, 1990), p. 28.
[40] W. Nazarewicz, J. Dobaczewski, T. R. Werner, J. A. Maruhn, P.-G. Reinhard, K. Rutz, C. R. Chinn, S. A. Umar, and M. R. Strayer, Phys. Rev. C **53**, 740 (1996).
[41] M. Rayet, M. Arnould, F. Tondeur, and G. Paulus, Astron. Astrophys. **116**, 183 (1982).
[42] J. Friedrich and P.-G. Reinhard, Phys. Rev. C **33**, 335 (1986).
[43] B. A. Brown, Phys. Rev. C **58**, 220 (1998).
[44] D. Guillemaud-Mueller, J. C. Jacmart, E. Kashy, A. Latimier, A. C. Mueller, F. Pougheon, A. Richard, Yu. E. Penionzhkevich, A. G. Artukh, A. V. Belozyorov, S. M. Lukyanov, R. Anne, P. Bricault, C. Détraz, M. Lewitowicz, Y. Zhang, Yu. S. Lyutostansky, M. V. Zverev, D. Bazin, and W. D. Schmidt-Ott, Phys. Rev. C **41**, 937 (1990).
[45] O. Tarasov, R. Allatt, J. C. Angelique, R. Anne, C. Borcea, Z. Dlouhy, C. Donzaud, S. Grevy, D. Guillemaud-Mueller, M. Lewitowicz, S. Lukyanov, A. C. Mueller, F. Nowacki, Yu. Oganessian, N. A. Orr, A. N. Ostrowski, R. D. Page, Yu. Penionzhkevich, F. Pougheon, A. Reed, M. G. Saint-Laurent, W. Schwab, E. Sokol, O. Sorlin, W. Trinder, and J. S. Winfield, Phys. Lett. B **409**, 64 (1997).
[46] T. Otsuka and N. Fukunishi, Phys. Rep. **264**, 297 (1996).
[47] Yao-song Shen and Zhongzhou Ren, Z. Phys. A **356**, 133 (1996).
[48] Z. Ren, W. Mittig, B. Chen, and Z. Ma, Phys. Rev. C **52**, R20 (1995).
[49] P. Möller, J. R. Nix, W. D. Meyers, and W. J. Swiatecki, At. Data Nucl. Data Tables **59**, 185 (1995).
[50] G. Audi, O. Bersillon, J. Blachot, and A. H. Wapstra, Nucl. Phys. **A624**, 1 (1997).
[51] R. Nayak and L. Sapathy, Nucl. Phys. **A304**, 64 (1978).
[52] B. Jonson and K. Riisager, Philos. Trans. R. Soc. London, Ser. A **356**, 2063 (1998).
[53] I. Tanihata, J. Phys. G **22**, 157 (1996).
[54] N. Fukunishi, T. Otsuka, and I. Tanihata, Phys. Rev. C **48**, 1648 (1993).
[55] I. Tanihata, D. Hirata, T. Kobayashi, S. Shimoura, K. Sugimoto, and H. Toki, Phys. Lett. B **289**, 261 (1992).
[56] J. Dobaczewski, H. Flocard, and J. Treiner, Nucl. Phys. **A422**, 103 (1984).
[57] H. Sakurai, N. Aoi, D. Beaumel, N. Fukuda, M. Hiroi, E. Ideguchi, M. Ishihara, H. Iwasaki, T. Kishida, T. Kubo, H. Kumagai, S. M. Lukyanov, T. Nakamura, M. Notani, Yu. Ts. Oganessian, Yu. E. Penionzhkevich, T. Teranishi, Y. Watanabe, Y. Watanabe, K. Yoneda, and A. Yoshida, Nucl. Phys. **A616**, 311c (1997).
[58] G. A. Lalazissis, D. Vretenar, W. Pöschl, and P. Ring, Phys. Lett. B **418**, 7 (1998).
[59] S. Raman, C. H. Malarkey, W. T. Milner, C. W. Nestor, and P. H. Stelson, At. Data Nucl. Data Tables **36**, 1 (1987).
[60] T. Motobayashi, Y. Ikeda, Y. Ando, K. Ieki, M. Inoue, N. Iwasa, T. Kikuchi, M. Kurokawa, S. Moriya, S. Ogawa, H. Murukami, S. Shimoura, Y. Yanagisawa, T. Nakamura, Y. Watanabe, M. Ishihara, T. Teranishi, H. Okuno, and R. F. Casten, Phys. Lett. B **346**, 9 (1995).
[61] G. A. Lalazissis, A. R. Farhan, and M. M. Sharma, Nucl. Phys. **A628**, 221 (1998).
[62] T. Suzuki, H. Geissel, O. Bochkarev, L. Chulkov, M. Golovkov, N. Fukunishi, D. Hirata, H. Irnich, Z. Janas, H. Keller, T. Kobayashi, G. Kraus, G. Münzenberg, S. Neumaier, F. Nickel, A. Ozawa, A. Piechaczeck, E. Roeckl, W. Schwab, K. Sümmerer, K. Yoshida, and I. Tanihata, Nucl. Phys. **A630**, 661 (1998).
[63] D. Hirata, H. Toki, T. Watabe, I. Tanihata, and B. V. Carlson, Phys. Rev. C **44**, 1467 (1991).
[64] B. A. Brown and W. A. Richter, Phys. Rev. C **58**, 2099 (1998).